

Nebular Abundance Errors

Jason Alexander and Bruce Balick

Astronomy Department, University of Washington, Seattle, WA 98195

Email: jalex@astro.washington.edu, balick@astro.washington.edu

ABSTRACT

The errors inherent to the use of the standard “ionization correction factor” (i_{CF}) method of calculating nebular conditions and relative abundances of H, He, N, O, Ne, S, and Ar in emission line nebulae have been investigated under conditions typical for planetary nebulae. The photoionization code CLOUDY was used to construct a series of model nebulae with properties spanning the range typical of PNe. Its radial “profiles” of bright, frequently observed optical emission lines were then summed over a variety of “apertures” to generate sets of emission line measurements. These resulting line ratios were processed using the i_{CF} method to “derive” nebular conditions and abundances. We find that for lines which are summed over the entire nebula the i_{CF} -derived abundances differ from the input abundances by $\leq 5\%$ for He and O up to $\leq 25\%$ or more for Ne, S, and Ar. For resolved observations, however, the discrepancies are often much larger and are systematically variable with radius. This effect is especially pronounced in low-ionization zones where nitrogen and oxygen are neutral or once-ionized such as in FLIERs, ansae and ionization fronts. We argue that the reports of stellar-enriched N in the FLIERs of several PNe are probably specious.

1. Introduction

Chemical abundances of gaseous nebulae are among the most frequently used astrophysical tools for measuring the rates of heavy element formation, inferring the history of star formation, and gauging the effects of internal stellar nucleosynthesis and mixing. In this paper we subject the most common method of measuring heavy element abundances, the “ionization correction factor” (i_{CF}) method, to a simple but rigorous examination.

The i_{CF} method was initially developed by Torres–Peimbert & Peimbert (1979) as a method for converting measured nebular emission line fluxes into chemical abundances. The application of the method is straightforward: Using standard diagnostic techniques,

the electron density, n , temperature, T , and the ionic abundances (relative to H^+) of species with visible lines (e.g. He^+ , He^{++} , N^+ , O^+ , O^{++} , Ne^{++} , S^+ , S^{++} , Ar^{++}) are derived from observed line ratios. Total chemical abundances are then derived by correcting the ionic abundances for unseen ionization stages using i_{CF} s.

The many untestable assumptions used to formulate these correction factors render them the weakest link in this methodology; however, the resulting errors have never been stringently assessed. Various statistical studies of nebulae have been used to refine the various correction factors of the i_{CF} method, the latest and most exhaustive study being that of Kingsburgh & Barlow (1994) (hereafter, KB). However, these studies all rely on observations of nebulae whose assumed chemical properties are based on i_{CF} techniques – a somewhat circular process. More recently, Henry *et al.* (1996), Kwitter & Henry (1996), and Kwitter & Henry (1997) have developed a method in which i_{CF} abundances are only used as a starting point for CLOUDY models (see Ferland *et al.* 1996 or Ferland *et al.* 1994 for a description of CLOUDY). Making certain assumptions about the nebular structure and stellar properties, Henry *et al.* (1996) vary the input abundances to CLOUDY until its predicted line ratios match their observed ones. They find that averaged over the nebula, i_{CF} abundances differ by $\leq 20\%$ from those used in their most successful CLOUDY models.

If this were the entire story then this paper would not have been submitted. However, Balick *et al.* (1994) observed several planetary nebulae (PNe) with $1''.5$ resolution along a slit. Using the i_{CF} method they derived radial increases in nitrogen abundances as high as a factor of 7, whereas other elemental abundances remain constant. In addition, Guerrero *et al.* (1995) have drawn similar conclusions about nitrogen variations in the bipolar nebula M1-75 while Corradi *et al.* (1997) found radial increases for helium, neon, sulfur, and argon in their long-slit studies of IC 4406. Based on such abundance variations with radius some authors have proposed the recent ejection of high-velocity, element-enriched material by the central star. If real, these interpretations suggest some bizarre stellar enrichment process for which no theoretical understanding exists.

Alternately, the i_{CF} -derived abundance gradients could be erroneous. Investigating this possibility is the goal of the present paper. As we shall see, CLOUDY simulations show that there are important regions, such as all low-ionization zones, in which the i_{CF} abundances of some elements can be highly discrepant (a factor of three or more). Other total abundances befall similar though less extreme fates.

2. Methodology

We denote elements by standard abbreviations, H, He, C, etc. Unless implied otherwise in context, we shall use the following abbreviations for specific emission lines: [NII] = [NII] λ 6583Å, [OI] = [OI] λ 6300Å, [OII] = [OII] λ 3727Å = [OII] $\lambda\lambda$ (3726 + 3729)Å, [OIII] = [OIII] λ 5007Å, [NeIII] = [NeIII] λ 3869Å, [ArIII] = [ArIII] λ 7136Å, [ArIV] = [ArIV] λ 4740Å, [ArV] = [ArV] λ 7005Å, [SII] = [SII] $\lambda\lambda$ (6717 + 6731)Å, and [SIII] = [SIII] λ 6312Å. Generally speaking, total abundances are relative to H and ionic abundances are relative to H⁺, so that “Ne” means the Ne/H abundance and “O⁺⁺” is equivalent to O⁺⁺/H⁺, etc. “Profile” implies the radial distribution of some quantity, e.g. an emission line profile. The electron density, $n(\text{S}^+)$, is determined using the 6717Å and 6731Å lines of S⁺ and the electron temperature is determined two ways; $T(\text{N}^+)$ using the [NII] 6583Å, 6548Å and 5755Å lines and $T(\text{O}^{++})$ using the [OIII] 4959Å, 5007Å and 4363Å lines using standard methods.

In the present study we used CLOUDY (version 90.02) in order to conduct a controlled study of i_{CF} -derived abundances and their sensitivity to changes in nebular conditions such as nebular geometry, stellar temperature, luminosity and emergent spectrum, and abundances. This procedure bypasses all observational problems (e.g. reddening corrections and flux calibrations) and does not rely on a statistical or empirical analysis of the observations of a heterogeneous sample of observed objects.

Based on a set of “*assumables*”, namely, the chemical abundances $A(X)$ relative to H, along with a nebular density structure, $n(\text{H}, r)$, and a standard star model, $Q_*(T_*, L_*)$ or $Q_*(T_*, g_*)$, CLOUDY was used to compute the profiles of the ionization structure, electron density, electron temperature, and the emissivities of bright optical lines. CLOUDY’s emissivity profiles were summed over different “apertures” to synthesize a set of “*observables*”, i.e. emission lines fluxes in relatively bright nebular lines.

The original profiles and these observables were normalized to H β and then used to determine a set of “*derivables*” (denoted with a prime) from ratios of observable lines – $n'(\text{S}^+)$, $T'(\text{N}^+)$, $T'(\text{O}^{++})$, and ionic abundances $A'(X_{ion})$ – using standard techniques. The expressions for this process were obtained by fits to output from the IONIC and TEMDEN tasks in the IRAF/STSDAS¹ program NEBULAR (Shaw & Dufour 1995). These fits, which are generally accurate to 2% or better, are listed in Appendix A. In all cases we used $T(\text{N}^+)$ and $T(\text{O}^{++})$ for computing the abundances of ions emitted from low- and high-ionization regions, respectively.

¹Image Reduction and Analysis Facility is distributed by National Optical Astronomy Observatories, which is operated by the Association of Universities for Research in Astronomy, Inc. under cooperative agreement with the National Science Foundation.

The derived ionic abundances, $A'(X_{ion})$, were used as input to the i_{CF} method used by KB in order to derive the resultant total abundances $A'(X)$. To this end, the $A'(X_{ion})$ are multiplied by certain i_{CF} corrections, $i_{CF}(X)$, which are based on geometric assumptions about the relative volumes occupied by the unseen ionization stages. Expressions for the i_{CF} correction factors for various atoms are also listed in the Appendix. Finally, the “discrepancy ratios”, $\mathcal{A}(X) \equiv A'(X)/A(X)$ are computed. (Note that our $\mathcal{A}(X) \equiv 1/\xi(X)$ of Henry *et al.* 1996).

As an example of this process, in many nebulae the dominant ionization stages of nitrogen are N^+ and N^{++} . Although N^+ emits several bright optical lines (rendering N^+/H^+ readily measurable), N^{++} does not. Hence we must estimate N by correcting N^+ with an i_{CF} where $i_{CF}(N) = N/N^+$, recalling of course that N is not directly measurable. In this case, the i_{CF} method assumes that both nitrogen and oxygen have the same ionization structure; i.e. the fractional ionizations $x(N^+) = x(O^+)$ and $x(N^{++}) = x(O^{++})$ at all radii. Thus $i_{CF}(N) = O/O^+$, where (O/O^+) can be derived from observables, as shown in Appendix A. Note that no explicit knowledge of the nebular physical conditions or the excitation source is required beyond that needed to determine ionic abundances.

Using this technique, an assessment of the global i_{CF} nebular abundances was made by integrating the line emissivity profiles computed by CLOUDY over four regions or apertures: the entire model nebula (truncated where $x(H^+) \leq 30\%$); a “high-ionization” region (in which $x(O^+ + O^o) < 50\%$), a “low-ionization” region (in which $x(O^+) \geq 50\%$), and a “neutral” region (in which $x(O^o) \geq 50\%$ and $x(H^+) \geq 30\%$). The high-ionization region is typical of density-bounded nebulae observed with a large aperture. The low-ionization and neutral regions are characteristic of low-ionization features, such as ansae and FLIERs, commonly found in planetary nebulae. The computations stop at $x(H^+) = 30\%$ since the assumptions of ionization and thermal equilibrium become poor at about that point and the use of CLOUDY is not appropriate. (Even at $x(H^+) \approx 50\%$ the detailed results are probably uncertain.)

The procedure was applied to a “baseline model” in which the total density is 0 cm^{-3} within a radius $R_o = 10^{17} \text{ cm}$, and 3000 cm^{-3} beyond it. Abundances $\log A(H:He:C:N:O:Ne:S:Ar) = 0.0 : -1.0 : -3.52 : -4.0 : -3.22 : -3.82 : -4.82 : -5.0$ were used. A star with $\log L_* = 37.4 \text{ (erg s}^{-1}\text{)}$ and a blackbody spectrum with temperature $\log T_* = 5 \text{ (}^\circ\text{K)}$ was adopted. This baseline model is representative of typical bright galactic planetary nebulae such as NGC 3242 and 7662.

Several input parameters were then varied in order to ascertain how the derived abundances $A'(X)$ and i_{CF} discrepancies $\mathcal{A}(X)$ are affected. The parameter variation studies are intended to explore reasonable ranges of structural and chemical conditions.

These parameter variation sets, Δ , are summarized in the left column of Table 1.

The ΔR_o sequence probes the effect of nebular geometry through changes in the size of the empty central cavity. For ΔO , ΔN , and $\Delta(N+O)$, abundances were varied to determine the extent to which nebular abundances affect the i_{CF} abundance discrepancies. We computed ten models, $\Delta(\log T_*, \log L_*)$, in which a “star” moves along a typical Harman–Seaton sequence in its PN evolution. That is, a range of stellar UV flux distributions (assumed to be blackbodies) and luminosities was considered. For comparison, we also considered seven nonLTE models, $\Delta(\log T_*, \log g_*)$, which were chosen to approximate models from the $\Delta(\log T_*, \log L_*)$ sequence to examine the effects of changes in the shape of the input spectrum. These nonLTE models are interpolations of a set of models from Klaus Werner (Werner *et al.* 1991) included in the CLOUDY package.

3. Results

The model–computed ionization structure and emission line profiles of the baseline model are shown in the top and center panels of Figure 1, respectively. The figure is characteristic of nearly all of the model nebulae. The resulting abundance discrepancies, $\mathcal{A}(X, r)$, are shown in the lower panel of Fig. 1. Shaded regions show the areas integrated for the low–ionization and neutral regions. Note that the differences between the ionization volumes for O^{++} and Ne^{++} and O^+ and N^+ are cross-hatched in the left and right panels, respectively.

The resultant radial profiles of $n'(S^+, r)$, $T'(N^+, r)$, $T'(O^{++}, r)$, and the ionic abundances $A'(X_{ion}, r)$ are found to be in such close agreement with their “real” counterparts computed by CLOUDY that we need not distinguish between them hereafter. This agreement is in spite of different atomic constants in the codes used in both methods which only serves to reassure us that the errors in the i_{CF} method are real and measurable. One exception is the Ar^{++} abundance determined from the 7136Å line for which IONIC’s results consistently differ from CLOUDY’s computed values by a factor of two. Other exceptions occur, but only in extreme circumstances.

3.1. Global i_{CF} abundances measurements.

The emission line profiles were integrated over each of the four types of regions (entire nebula, high–ionization, low–ionization, and neutral) using both volume and line–of–sight weighting. These results mimic observations using apertures that isolate and average over

the corresponding volumes or lines of sight. From these integrated observables $n'(\text{S}^+)$, $T'(\text{N}^+)$, $T'(\text{O}^{++})$, $A'(X_{ion})$, the i_{CF} correction factors, the derived abundances $A'(X)$, and i_{CF} abundance discrepancies $\mathcal{A}(X)$ were derived for each zone separately.

A grid of the line flux ratios integrated over the full nebular volume and corresponding to each of the present model sequences is presented in Table 1. The nebular $\text{H}\beta$ luminosity and radius for each model (relative to the baseline) are tabulated, as are the densities and temperatures that would be derived directly from full-volume integrated emission line ratios.

It is interesting to note how the brightnesses of all of the low-ionization lines increase (relative to $\text{H}\beta$) along the Harman–Seaton sequence through all ten of the $\Delta(\log T_*, \log L_*)$ models. By the end of this sequence, the $[\text{NII}]/\text{H}\alpha$ line ratio exceeds 1.5 (assuming a standard Balmer decrement value of 2.8 for the $\text{H}\alpha/\text{H}\beta$ line ratio). Similarly, $[\text{OI}]/\text{H}\alpha$ approaches 25%. These are global integrated values, not just local ones near the nebular edge. Comparing these resulting flux ratios to shock models, we note that pure photoionization models can give rise to low-ionization line strengths comparable to many planar shock models with shock velocities $\leq 200 \text{ km s}^{-1}$ (e.g. Hartigan *et al.* 1994). Within the potential uncertainties of abundances determined with i_{CF} methods, the line ratios in the low-ionization portion of a planetary nebula can not reliably be distinguished from shock models without additional information.

The $\text{H}\beta$ luminosities are relevant for studies of the PN luminosity function. In the case that the nebulae are ionization bounded, these luminosities are insensitive to the assumed nebular geometry or abundances (see Table 1). However, as expected, they are excellent discriminators of the ultraviolet photon flux of the central star, i.e. its evolutionary state.

The nebular densities and temperatures in Table 1 exhibit some curious features. The $[\text{SII}]$ lines are weighted in favor of regions that are typically only partially ionized. Consequently $n(\text{S}^+)$ underestimates the true nebular electron density (3300 cm^{-3} in this case) by more than 20%. In addition, $T(\text{N}^+)$ can differ from $T(\text{O}^{++})$ by more than 1000 °K ($\sim 10\%$) due to changes in the nebular temperature profile through the N^+ and O^{++} regions. Accordingly, observed $T(\text{N}^+)$ and $T(\text{O}^{++})$ can be expected to differ in real nebulae in which no small-scale temperature fluctuations occur (cf Fig. 1). The sign of the $T(\text{N}^+) - T(\text{O}^{++})$ temperature difference reverses at stellar temperatures around 10^5 °K .

On the one hand, abundance errors are exacerbated unless $T(\text{N}^+)$ and $T(\text{O}^{++})$ are used for the computation of low- and high-ionization species, respectively. On the other hand, the errors which derive from problems in measuring $n'(\text{S}^+)$, $T'(\text{N}^+)$ and $T'(\text{O}^{++})$ are often small compared to other potential problems which are inherent to the i_{CF} method.

A key assumption in the i_{CF} method is that the ionization structure of N and O (and hence N^+ and O^+) is identical. However, as seen in Fig. 1, *these ionization zones are obviously not cospatial!* Although charge transfer locks O^+ to H^+ , charge transfer is far less important in the ionization structure of N^+ (Osterbrock 1989). Hence the ionization structures of N^+ and O^+ are only weakly coupled. Similarly, the ionization fractions He^+ , O^{++} , and Ne^{++} are assumed to be roughly equal in the i_{CF} method. In the CLOUDY models these deviate from one another, especially near the edge of the high-ionization region. Here too, charge transfer affects O^{++} to a greater degree than Ne^{++} . These potential errors in the i_{CF} method have long been recognized (e.g. Péquignot *et al.* 1978).

The substantive issue in this paper is a quantitative analysis of their effect on i_{CF} abundances, i.e. the magnitude of the discrepancy, $\mathcal{A}(X)$. The results of $\mathcal{A}(X)$ are summarized in Table 2 for the ΔR_o and $\Delta(\log T_*, \log L_*)$ sequences of models. Results for the ΔO , ΔN , $\Delta(N + O)$ sequences show only small departures from those of the baseline model and are not shown. Similarly, the nonLTE model atmospheres don’t change the resulting i_{CF} abundances to any great degree. In general, the new discrepancies differ from the blackbody case by $\leq 5\%$ for unresolved nebulae and $\leq 7\%$ for resolved observations. In cases where the blackbody abundances were good (discrepancies $\leq 5\%$) the nonLTE result tends to differ by $\leq 2\%$.

Several interesting conclusions can be drawn from inspection of the table. The abundances derived for He, N, and O from entire-volume observations (i.e., large-aperture observations of ionization bounded nebulae) are generally good. A similar result was found by Henry *et al.* (1996). S and Ar are generally not fitted well (errors $> 20\%$) with Ar systematically overestimated by $> 20\%$ in volume integrals. Errors for Ne can exceed 50% or more and vary greatly with the properties of the central star.

But the apparent accuracy of the i_{CF} method can be deceptive. Note in Fig. 1 the degree to which $\mathcal{A}(X, r)$ varies with radius. In a volume-average over the entire nebula, these variations tend to cancel; however, many of the local values of $\mathcal{A}(X, r)$ deviate from unity. In regions of low ionizations the i_{CF} discrepancies of He, N, Ne, and Ar often approach 20%, and sometimes even exceed 100%. Local i_{CF} abundance discrepancies are considered in §§3.2 and 3.3.

3.2. Radial i_{CF} abundance measurements in the baseline model

We next consider the abundances derived from observations in which the baseline nebula is spatially resolved. Refer to Fig. 1 and the baseline model results shown in Table 2.

In the outer parts of the nebula where the i_{CF} approximation $N/O = N^+/O^+$ breaks down, $\mathcal{A}(N)$ increases from 0.7 in the nebular interior to 2 in the neutral zone. If the emission lines of the baseline model were observed using a long slit, *the use of the i_{CF} approximation would lead to the erroneous conclusion that both N/O and N/H increase by a factor of three or more!*

The abundances determined solely or largely from lines of high ionization, He and Ne, also show large discrepancies in low-ionization regions; however, unlike [NII], only a small fraction of the helium and neon line fluxes arise outside the high-ionization zone. Therefore the magnitude of the abundance discrepancy will not be noticeable in practice. Nonetheless, i_{CF} abundance errors in He and Ne will certainly arise in isolated low-ionization ansae, lobes, or halos.

Similarly, the derived abundances of S and Ar using only the standard [SII] and [ArIII] lines are affected. However, their i_{CF} discrepancies can be ameliorated if lines of [SIII] and [ArIV] are detected and included in the i_{CF} abundance analysis.

Clearly, except for O, all i_{CF} abundances are vulnerable to large systematic errors with nebular radius, especially in or near the ionization front. This is particularly apparent in the lower panel of Fig. 1.

3.3. Radial i_{CF} abundance measurements for other models

The i_{CF} discrepancies for other models show some interesting trends from region to region. Here we point out only a few of them. Consider first the ΔR_o sequence. As the radius of the central hole grows and the impinging stellar radiation becomes more dilute (i.e. the ionization parameter decreases), the relative size of the low-ionization zone grows and the boundary between the high- and low-ionization regions becomes less distinct. This has a profound effect on abundances measured in the high-ionization zone, as seen in Table 2. Hollow PNe such as Abell 39 and halos such as NGC 6826, ionized by highly dilute stellar radiation, are likely to be the most affected.

Consider the $\Delta(\log T_*, \log L_*)$ sequence. Abundance discrepancies are very sensitive to the assumed temperature of the excitation source, as is easily seen in Table 2. The first model in the sequence represents a cool stellar ionizing source, $\log T_* = 4.55$. In this case the high-ionization zone occupies less than half of the nebular volume, and the boundary between it and the low-ionization zone is not sharply defined. In this transition region the various $\mathcal{A}(X)$'s are large. Only oxygen, for which both important ionization stages are visible, has a reliably measurable abundance. This serves as a warning for abundance

measurements of HII regions as well as low-ionization PNe such as IC418 and BD+30°3639.

As the stellar temperature increases in the sequence the ionization patterns seen in Fig. 1 are quickly established. The low-ionization zone becomes smaller in radius, and the lines that are emitted from it drop in overall importance. As a result, the abundance discrepancies $\mathcal{A}(X)$ are closest to unity for the second through fifth models in the sequence.

As the stellar luminosity drops (seventh through tenth models), the low-ionization zone again fills more of the nebular volume. Correspondingly, the $\mathcal{A}(X)$ ’s increase. As discussed earlier, the emission line ratios of low-ionization species such as O^0 , S^+ , O^+ , N^+ , and Ar^{++} resemble values found in low-velocity shocks (Hartigan *et al.* 1994). At the same time, high-ionization lines from He^+ , He^{++} , O^{++} , and Ne^{++} remain bright. Except for oxygen, the ionization correction factors become large and the corresponding abundance discrepancies mount.

4. Discussion

Ionization correction techniques have long been used in both galactic and extra-galactic astronomy. As early as 1985, Bob Rubin recognized problems with derived nitrogen abundances. Our work bears out his assertions. We confirm that as electron temperature drops the ratio N^{++}/O^{++} rises.

While the present models focus on PNe, the i_{CF} abundance discrepancies are important for observations of galactic and extragalactic HII regions (Gonzalez-Delgado *et al.* 1994, Martin 1996, and Storchi-Bergmann *et al.* 1996 to name only a few recent examples). Storchi-Bergmann *et al.* (1996), in their examination of the central regions of AGNs, assume that i_{CF} assumptions can lead to an under-estimate in the nitrogen abundance of 20%; however, our results suggest that the discrepancy could be 40–50% based on the nebular temperatures and densities that they find.

Nitrogen in radiation-bounded objects like planetary nebulae can be easily overestimated, particularly in lines of sight that largely or exclusively sample the low-ionization portion of the nebula where the N^+ profile extends beyond both those of H^+ and O^+ . A slit which lies across an ionization-bounded nebula should clearly show a rise in N relative to both O and H due to the form of the i_{CF} for nitrogen. This effect certainly contributes to the results of Balick *et al.* (1994) and Guerrero *et al.* (1995), although it is unclear whether or not it can completely account for the reported variation in N/O. Similar, although less pronounced, problems with Ne and S also exist. Surprisingly, the recent results of Corradi *et al.* (1997) show the expected radial increase in all species *except*

nitrogen. These radial abundance discrepancies will be exaggerated for highly extended nebulae such as bipolars in which the flux of radiation striking most of the lobe walls is both dilute and incident at high obliquity (see the values for the ΔR_o series in Table 2).

Since 1967, Peimbert, Torres–Peimbert and their collaborators have been examining the physical effects of both large– and small–scale temperature fluctuations on abundances determined by the i_{CF} method. Recently, Peimbert *et al.* (1995b) used emission line temperatures from different elements to attempt to measure the temperature fluctuations in 17 Type I PNe. To quantify the fluctuations, they measured temperatures for numerous emission lines and compared them to one another. Our work clearly shows that this is not a sound test as the lines originate at different points in the nebula due to different sensitivity to temperatures and densities. An examination of the temperatures in Table 3 of Peimbert *et al.* (1995b) shows that roughly half of the objects (notably including all of the Minkowski objects in their sample) have $T(\text{N}^+) - T(\text{O}^{++})$ values that are within the differences that one should expect to measure in a smooth, homogeneous PN with no small–scale temperature fluctuations.

Recently, a puzzling factor–of–three–to–five disagreement in the oxygen abundances measured from forbidden and recombination lines has arisen (Liu & Danziger 1993, Peimbert *et al.* 1993, Liu *et al.* 1995, Mathis 1995). The present study shows that O abundances measured using the i_{CF} method are generally accurate to $\sim 5\%$ measured globally, and 10% measured with a pencil beam near the nebular center (before observational errors). Thus our results do not resolve this controversy.

5. Conclusions

The present model results show that use of i_{CF} techniques for abundance analysis for spatially unresolved objects gives results accurate to $\sim 20\%$ as found by Henry *et al.* (1996). Larger discrepancies can occur for some nebular conditions including cool ionization sources or highly dilute incident stellar UV radiation.

For spatially resolved nebulae, i_{CF} abundance errors can be high locally, especially for N, Ne, and Ar in or near an ionization front. These errors have led to probable overestimates of N/O abundance variations in FLIERs and bipolar PNe.

Further, the emission line ratios predicted for the low–ionization species in or near ionization fronts in resolved observations resemble those predicted for shocks. This is the cause of some ambiguity, if not confusion, in the interpretation of line ratios.

The magnitudes of errors in the i_{CF} method differ for nebulae of various sizes and excitation/ionization sources. In addition, the i_{CF} errors depend on the extent to which ionizing photons are absorbed or escape (i.e. whether the nebula is ionization or density bounded). Consequently, statistical studies of abundances in many objects need to account for these types of conditions.

Nebulae excited by stars with $T_* \leq 45000^\circ\text{K}$ have relatively large i_{CF} discrepancies. Our work has concentrated on conditions typical in PNe and thus suggests that a detailed study of i_{CF} abundances in galactic and extragalactic HII regions needs to be undertaken in order to assess the veracity of i_{CF} -derived abundances and gradients in the disks of spiral galaxies.

It is a pleasure to thank the developer of CLOUDY, Gary Ferland. This research was sponsored by NSF grant AST 9417112 and NASA GO-6117.

A. Empirical Procedures for Deriving Abundances

A.1. Densities and Temperatures

Straightforward analytical expressions can be used to derive densities, temperatures and ionic abundances from the measured emission line ratios. The functions shown below were obtained by a linear least-squares fit to a series of results from the IONIC and TEMDEN tasks in the IRAF/STSDAS software package. $I\lambda$ or $I(\lambda\lambda)$ is the measured intensity of a line relative to $H\beta = 1$ (not 100) after correction for reddening.

The task TEMDEN in the nebular package in IRAF returns a value of density or temperature for a specific set of diagnostic line ratios. The density formula is computed assuming $T = 10^4$ °K and is valid for $100 < n(\text{cm}^{-3}) < 30000$. Assuming that the atomic data are correct, the errors of the fits for $n(\text{S}^+)$ and $n(\text{Cl}^{++})$ are typically 5% or less. Those for $n(\text{Ar}^{+++})$ are about 8%. As in the paper above, X^+ implies X^+/H^+ and X implies X/H .

$$\log[n(\text{S}^+)] = 21.683 - 41.177r + 39.848r^2 - 13.954r^3 \quad \text{where } r = \frac{I6717}{I6731}$$

$$\log[n(\text{Cl}^{++})] = 14.775 - 19.036r + 20.275r^2 - 8.3713r^3 \quad \text{where } r = \frac{I5517}{I5538}$$

$$\log[n(\text{Ar}^{+++})] = 12.713 - 5.7379r - 5.9903r^2 + 14.375r^3 - 7.1339r^4 \quad \text{where } r = \frac{I4711}{I4740}$$

The temperature formulae are computed assuming $n = 10^3 \text{cm}^{-3}$ and are valid for $6000 < T(\text{°K}) < 17000$. Errors are less than 1%.

$$\log[T(\text{N}^+)] = 5.96r^{-0.387} + 8.13 \quad \text{where } r = \frac{I(6548 + 6583)}{I5755}$$

$$\log[T(\text{O}^{++})] = 5.22r^{-0.304} + 8.185 \quad \text{where } r = \frac{I(4959 + 5007)}{I4363}$$

Normally some quality-weighted average value of n and T are adopted before proceeding further. However, if the data are good, then values of n and T can be used which are optimized for the ionization potentials of the ions in the expressions below.

A.2. Ionic Abundances

Ionic abundances of He are computed from expressions fitted to effective recombination coefficients found in Osterbrock (1989) (Tables 4.4, 4.5, and 4.6). A density of $n = 10^4 \text{cm}^{-3}$ has been assumed. We acknowledge that recent work (e.g. Smits 1996) has provided better coefficients for helium, however since our goal is to identify errors in the method,

rather than differences in atomic coefficients, we have chosen to use Osterbrock’s values which match those used in CLOUDY. The deviation from curves fit to Osterbrock’s tables is smaller than 5%.

The task IONIC in the nebular package in IRAF was used to compute various ionic abundances from forbidden line ratios (relative to $H\beta$) at $T = 7500, 10000, 12500$, and 15000 °K for each of the following densities: 30, 100, 300, 1000, 3000, 5000, 10000, 15000, 20000, 25000, and 30000 cm^{-3} . Empirical expressions for N, O, Ne, S, and Ar isotopes whose coefficients (including those inside the exponentials) are determined from a least-squares fit to IONIC’s results as well as those for He appear in Table 3. These fits are not accurate outside of the ranges of temperature and density above.

In Table 3, $x = n/\sqrt{T}$ and line ratios are all relative to $H\beta = 1$, not 100. To the right side of the fits, residuals of the fit are shown at 7500, 10000, 12500, and 15000 °K, respectively, as a percentage of the fitted value.

A.3. Total abundances

The ionic abundances are multiplied by ionization correction factors to derive total abundances. The primary source for the expressions in Table 4 is Kingsburgh & Barlow (1994; KB). Alternate sources of ionization correction factors include Köppen *et al.* (1991; KAS), Peimbert *et al.* (1995b; PLTP) and Freitas-Pacheco *et al.* (1995; F-PBCI).

REFERENCES

- Balick, B. *et al.* 1994, ApJ, 424, 800
- Barker, T. 1980, ApJ, 240, 99
- Barlow, M. J. private communication
- Butler, S. E. *et al.* 1979, ApJ, 230, L59
- Corradi, R. L. M. *et al.* 1997, A&A, in press
- Ferland, G. J. *et al.* 1994, MNRAS, 266, 399
- Ferland, G. J. 1996, in HAZY, Univ. Kentucky Dept. Phys. & Astron. Internal Rep.
- Ferland, G. J. *et al.* 1996, Sixth Annual Conference on Astronomical Data Analysis Software and Systems (ADASS VI). Charlottesville, VA USA, ASP in press.

- de Freitas–Pacheco, J. A. *et al.* 1993, A&A, 271, 429
- Gonzalez–Delgado, R. M. *et al.* 1994, ApJ, 437, 239
- Gruenwald, R., and Viegas, S. M. 1995, A&A, 303, 535
- Guerrero, M. A. *et al.* 1995, ApJ, 444, L49
- Hartigan, P. *et al.* 1987, ApJ, 316, 323
- Hartigan, P. *et al.* 1994, ApJ, 436, 125
- Hawley, S. A., and Miller, J. S. 1977, ApJ, 212, 94
- Hawley, S. A., and Miller, J. S. 1978, PASP, 90, 39
- Henry, R. B. C. *et al.* 1996, ApJ, 458, 215
- Kingdon, J. B., and Ferland, G. J. 1995, ApJ, 450, 691
- Kingsburgh, R. L., and Barlow, M. J. 1994, MNRAS, 271, 257 (KB)
- Köppen, J. *et al.* 1991, A&A, 248, 197
- Kwitter, K. B., and Henry, R. B. C. 1996, ApJ, 473, 304
- Kwitter, K. B., and Henry, R. B. C. 1997, in preparation
- Liu, X–W., and Danziger, J. 1993, MNRAS, 263, 256
- Liu, X–W. *et al.* 1995, MNRAS, 272, 369
- Martin, C. L. 1996, ApJ, 465, 680
- Mathis, J. S. 1995, RMxAA Conference Series, 3, 207
- Osterbrock, D. E., Astrophysics of Gaseous Nebulae and Active Galactic Nuclei, Mill Valley, CA: University Science Books, 1989
- Peimbert, M. *et al.* 1993, ApJ, 414, 626
- Peimbert, M. *et al.* 1995a, RMxAA, 31, 131
- Peimbert, M. *et al.* 1995b, RMxAA, 31, 147
- Péquignot, D. *et al.* 1978, A&A, 63, 313

- Péquignot, D. 1980, A&A, 81, 356
- Rubin, R. H. 1985, ApJS, 57, 349
- Shaw, R. A., and Dufour, R. J. 1995, PASP, 107, 896
- Smits, D. P. 1996, MNRAS, 278, 683
- Storchi-Bergmann, T. *et al.* 1996, ApJ, 460, 252.
- Torres-Peimbert, S., and Peimbert, M. 1979, RMxAA, 4, 341
- Werner, K. *et al.* 1991, A&A, 244, 437

Fig. 1.— The ionization structure (upper panels; from CLOUDY 90.02), line emissivities (middle panels) and i_{CF} -derived abundance discrepancy (lower panel) for the baseline model. The shaded regions are zones where O^0 , O^+ , O^{++} and higher ionization species dominate, respectively. The inner edge of the nebula is at 10^{17} cm.

Cross hatching in the upper left panel shows deviations from the i_{CF} assumption that O^{++} and Ne^{++} are cospatial. Similarly, cross hatching in the upper right panel indicates deviations from the assumption that N^+ and O^+ are cospatial. In the lower panel, notice the tendency for the discrepancies to cancel when integrated over large radii or volumes. This implies that i_{CF} abundances are more likely to be specious when sampled through smaller apertures.

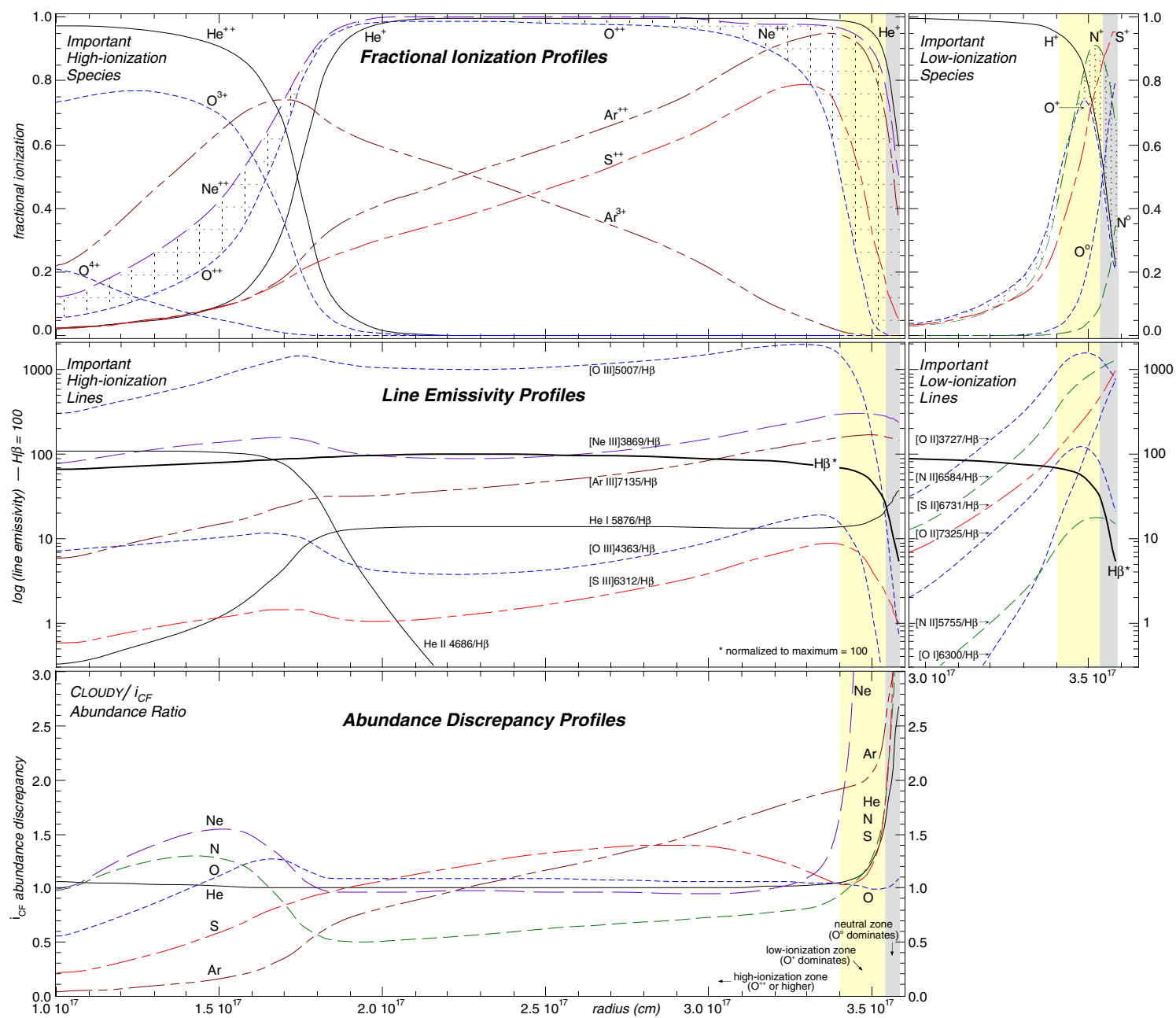


Table 1. Line intensities (relative to H β = 100), H β fluxes (baseline = 1), and nebular radii (baseline = 1) over entire nebular volume for the various models.

Changes from baseline model	He I 5876	He II 4686	[N I] 5200	[N II] 6584	[O I] 6300	[O II] 3727	[O II] 7325	[O III] 5007	[Ne III] 3869	[S II] 6717	[S II] 6731	[S II] 6312	[Ar III] 7135	[Ar IV] 4740	[Ar IV] 7005	L(H β) (case B)	neb. radius	nebular n(S ⁺)	volume T(N ⁺)	average T(O ⁺⁺)
log (T _* (BB), L _*) =																				
4.55,37.4	9.9	0.01	0.15	123	1.20	148	5.57	85.3	3.36	12.6	20.4	0.92	23.8	0.13	0.00	0.62	0.78	3534	7473	6685
4.70,37.4	14.4	0.19	0.20	58.7	2.29	114	6.12	389	34.4	8.49	13.5	1.49	50.0	3.33	0.00	0.97	0.90	3213	8858	7481
4.85,37.4	13.9	2.02	0.45	62.6	5.65	136	9.43	818	98.8	13.5	20.8	2.43	63.7	18.8	0.09	1.08	0.98	2754	10355	8777
5.00,37.4	12.7	10.0	0.85	82.0	9.04	184	14.2	1285	156	20.5	31.3	3.51	76.0	46.2	1.96	1	1	2644	11114	10112
5.15,37.4	10.4	28.4	1.21	103	11.8	234	18.7	1625	208	26.7	40.8	4.62	85.3	68.2	5.78	0.83	0.99	2649	11431	11404
5.25,37.1	8.36	45.7	1.99	141	16.9	318	25.9	1781	240	36.9	56.1	6.18	95.6	77.5	7.50	0.36	0.77	2599	11528	12543
5.25,36.6	8.46	46.8	3.26	195	24.6	431	34.7	1786	264	51.0	77.2	7.38	114	75.4	5.34	0.11	0.55	2555	11467	12524
5.20,36.1	9.79	38.7	5.07	271	34.9	576	44.8	1551	256	70.5	106	7.22	132	33.3	0.65	0.039	0.42	2532	11199	11667
5.05,35.6	12.8	16.4	6.59	341	41.3	655	44.6	743	168	82.4	124	4.43	114	3.98	0.01	0.015	0.35	2536	10342	9977
5.00,35.1	14.4	8.81	13.0	488	66.8	814	49.4	195	128	123	183	2.85	105	0.43	0.00	0.005	0.31	2369	9759	9553
log R ₀ = 16.3	12.7	10.0	0.84	80.8	8.93	182	14.0	1279	158	20.2	30.9	3.45	74.9	45.5	2.06	1.00	0.99	2642	11121	10098
16.7	12.7	10.0	0.83	80.9	8.90	182	14.0	1282	155	20.2	30.9	3.46	75.0	45.6	2.08	1.00	0.99	2650	11123	10102
17.0	12.7	10.0	0.85	82.0	9.04	184	14.2	1285	156	20.5	31.3	3.51	76.0	46.2	1.96	1	1	2644	11114	10112
17.3	12.7	10.6	0.95	89.5	9.79	199	15.2	1268	157	22.2	33.8	3.76	81.1	40.6	0.90	1.00	1.05	2655	11055	10059
17.7	12.8	12.2	2.22	171	18.1	357	25.5	1034	152	40.7	62.2	4.35	99.6	12.0	0.05	1.00	1.56	2673	10601	9474
log N = -0.7	12.7	10.0	0.18	17.1	9.69	196	15.4	1308	161	21.4	32.5	3.62	77.3	45.6	1.97	1.00	1.00	2616	11285	10186
-0.3	12.7	10.0	0.44	42.2	9.44	191	14.9	1298	159	21.1	32.1	3.57	76.8	46.4	1.97	1.00	1.00	2625	11221	10158
0.0	12.7	10.0	0.85	82.0	9.04	184	14.7	1285	156	20.5	31.3	3.51	76.0	46.2	1.96	1	1	2644	11114	10112
+0.3	12.8	10.1	1.53	155	8.16	170	12.8	1257	151	19.3	29.6	3.38	74.3	45.7	1.96	0.99	0.99	2702	10902	10023
+0.7	12.8	10.1	3.12	328	6.16	133	9.19	1181	136	16.4	25.3	3.03	69.7	44.2	1.92	0.98	0.98	2804	10246	9986
log O = -0.7	12.3	10.0	1.08	112	2.31	58.4	5.20	507	321	27.8	42.3	7.45	118	83.1	2.70	1.02	1.06	2623	12092	12285
-0.3	12.5	10.0	0.97	98.1	5.23	121	10.1	947	234	24.5	37.3	5.38	97.4	64.7	2.40	1.01	1.03	2640	11669	11241
0.0	12.7	10.0	0.85	82.0	9.04	184	14.2	1285	156	20.5	31.3	3.51	76.0	46.2	1.96	1	1	2644	11114	10112
+0.3	13.1	10.2	0.68	61.9	14.1	241	16.4	1504	88.2	15.6	23.8	1.93	53.7	27.8	1.28	0.99	0.95	2665	10336	8857
+0.7	13.7	10.7	0.40	34.8	19.6	267	14.0	1526	32.2	8.80	13.5	0.69	29.5	10.2	0.25	0.93	0.88	2740	9014	7515
log NO = -0.7	12.3	10.0	0.22	23.1	2.43	61.7	5.57	517	329	28.8	43.8	7.67	120	84.3	2.72	1.03	1.07	2621	12261	12380
-0.3	12.5	10.0	0.50	50.5	5.46	125	10.6	957	239	25.1	38.2	5.48	98.4	65.2	2.41	1.01	1.04	2619	11773	11292
0.0	12.7	10.0	0.85	82.0	9.04	184	14.2	1285	156	20.5	31.3	3.51	76.0	46.2	1.96	1	1	2644	11114	10112
+0.3	13.1	10.1	1.27	117	12.9	223	14.6	1476	85.2	14.8	22.6	1.86	52.6	27.6	1.28	0.97	0.95	2697	10124	8784
+0.7	13.7	10.6	1.52	143	13.8	199	9.24	1437	28.1	7.20	11.2	0.61	27.6	9.84	0.26	0.92	0.87	2895	8385	7376
log (T _* , g) _{NLTE} =																				
5.00,5.36	12.6	10.2	1.12	104	12.3	236	18.9	1657	209	26.4	40.1	4.29	84.8	65.4	2.19	0.90	0.99	2603	11468	10836
5.15,5.96	9.47	35.7	1.42	120	14.1	273	22.3	1829	235	31.2	47.5	5.38	90.8	76.1	6.37	0.74	0.97	2631	11568	12158
5.25,6.66	8.04	48.4	2.28	159	19.8	362	30.0	1968	264	40.6	61.6	7.04	102	79.5	7.04	0.32	0.76	2592	11678	13156
5.25,7.16	8.30	48.6	3.89	222	29.4	494	40.9	1990	294	57.2	86.2	8.43	123	77.5	5.20	0.10	0.54	2528	11657	13083
5.20,7.46	10.1	36.8	5.91	313	42.3	677	54.2	1735	294	81.3	123	8.14	144	32.9	0.55	0.036	0.42	2509	11425	12120
5.05,7.36	14.8	2.36	8.87	418	59.6	818	57.6	791	214	104	155	5.00	127	3.21	0.00	0.014	0.35	2412	10693	10305
5.00,7.66	16.3	0.28	19.0	607	106	1040	66.2	216	193	165	240	3.36	124	0.41	0.00	0.004	0.31	2369	9759	9553

* The input parameters for baseline model (shown in boldface) are: log₁₀ abundances H:He:C:N:O:Ne:S:Ar = 0:-1:-3.52:-4:-3.22:-3.82:-4.82:-5; density = 0 (3000) cm⁻³ within (beyond) R₀ = 10¹⁷ cm; central star: log L_{*} = 37.4 (erg s⁻¹), blackbody spectrum at log T_{*} = 5 (°K). The resulting baseline values of log L(H β) erg s⁻¹ = 35.36 and log nebular radius (cm) = 17.55.

Table 2. Abundance discrepancies for the grid of models.

ZONE VOLUME INTEGRAL ^{*,†}							ZONE LINE INTEGRAL ^{*,†}						
Model	He/H	N/H	O/H	Ne/H	S/H	Ar/H	He/H	N/H	O/H	Ne/H	S/H	Ar/H	
ENTIRE NEBULA: (x(H ⁺) > 30%)													
log R _O =16.3	1.03	0.98	0.91	0.98	0.85	1.27	1.01	0.78	0.74	0.79	0.52	0.70	
16.7	1.03	0.97	0.91	0.98	0.85	1.27	1.01	0.80	0.77	0.81	0.56	0.76	
17.0	1.03	0.98	0.91	0.99	0.86	1.28	1.02	0.86	0.82	0.87	0.65	0.88	
17.3	1.03	1.00	0.93	1.03	0.92	1.38	1.02	0.95	0.91	0.98	0.87	1.20	
17.7	1.04	1.07	1.01	1.36	1.10	1.83	1.04	1.06	1.02	1.34	1.10	1.82	
log (T _{*,L_*}) =													
4.55,37.4	0.67	0.78	0.96	0.48	1.35	1.37	0.80	0.71	0.99	0.53	1.26	1.66	
4.70,37.4	0.99	0.73	0.96	0.95	1.29	1.95	0.99	0.73	1.01	0.94	1.33	1.84	
4.85,37.4	1.01	0.90	0.93	1.01	1.08	1.55	1.01	0.86	0.92	0.96	1.00	1.26	
5.00,37.4	1.03	0.98	0.91	0.99	0.86	1.28	1.02	0.86	0.82	0.87	0.65	0.88	
5.15,37.4	1.03	1.02	0.92	0.98	0.73	1.09	1.02	0.88	0.81	0.81	0.52	0.69	
5.25,37.1	1.05	1.10	0.96	1.02	0.70	1.01	1.03	0.99	0.88	0.87	0.55	0.68	
5.25,36.6	1.07	1.22	1.05	1.22	0.82	1.21	1.05	1.19	1.04	1.13	0.76	1.00	
5.20,36.1	1.08	1.34	1.15	1.55	1.01	1.62	1.07	1.34	1.18	1.47	1.00	1.56	
5.05,35.6	1.08	1.19	1.06	2.17	1.12	1.99	1.07	1.17	1.07	2.05	1.11	1.97	
5.00,35.1	1.13	1.18	1.00	6.05	1.18	2.03	1.12	1.17	1.00	5.85	1.17	2.02	
HIGH-IONIZATION ZONE: (x(O ²⁺) > 50%)													
log R _O =16.3	1.01	0.71	0.91	0.88	0.94	1.17	1.00	0.57	0.74	0.74	0.57	0.65	
16.7	1.01	0.70	0.91	0.87	0.94	1.16	1.00	0.58	0.76	0.76	0.61	0.70	
17.0	1.01	0.71	0.91	0.88	0.94	1.18	1.01	0.63	0.82	0.81	0.71	0.82	
17.3	1.01	0.72	0.94	0.91	1.02	1.28	1.01	0.70	0.92	0.90	0.96	1.12	
17.7	1.01	0.80	1.07	1.09	1.15	1.69	1.01	0.81	1.07	1.09	1.16	1.69	
log (T _{*,L_*}) =													
4.55,37.4	0.99	0.35	1.15	0.63	1.15	2.06	0.99	0.35	1.15	0.66	1.17	2.06	
4.70,37.4	0.99	0.51	1.08	0.94	1.25	1.88	0.99	0.50	1.09	0.95	1.27	1.78	
4.85,37.4	1.00	0.62	0.96	0.91	1.15	1.45	1.00	0.60	0.95	0.91	1.04	1.20	
5.00,37.4	1.01	0.71	0.91	0.88	0.94	1.18	1.01	0.63	0.82	0.81	0.71	0.82	
5.15,37.4	1.01	0.77	0.92	0.86	0.79	0.99	1.01	0.67	0.80	0.75	0.57	0.62	
5.25,37.1	1.02	0.87	0.97	0.89	0.76	0.89	1.02	0.80	0.89	0.80	0.60	0.60	
5.25,36.6	1.02	1.02	1.11	1.06	0.92	1.06	1.02	1.03	1.10	1.03	0.88	0.89	
5.20,36.1	1.02	1.15	1.27	1.31	1.11	1.51	1.02	1.19	1.30	1.31	1.12	1.47	
5.05,35.6	1.01	0.98	1.21	1.43	1.09	1.79	1.01	0.98	1.22	1.43	1.09	1.79	
5.00,35.1	1.02	1.00	1.13	3.75	1.00	1.84	1.02	1.00	1.13	3.75	1.00	1.84	
LOW-IONIZATION ZONE: (x(O ⁺) > 50%)													
log R _O =16.3	1.18	1.20	1.01	3.95	1.10	1.94	1.17	1.19	1.01	3.90	1.10	1.94	
16.7	1.17	1.18	1.01	3.59	1.09	1.93	1.16	1.18	1.01	3.55	1.09	1.94	
17.0	1.18	1.19	1.01	3.90	1.10	1.94	1.17	1.19	1.01	3.85	1.10	1.94	
17.3	1.16	1.17	1.01	3.57	1.09	1.94	1.16	1.17	1.01	3.52	1.09	1.94	
17.7	1.13	1.11	1.01	3.50	1.09	1.98	1.13	1.11	1.01	3.47	1.09	1.98	
log (T _{*,L_*}) =													
4.55,37.4	0.57	0.80	0.96	0.40	1.34	1.12	0.66	0.75	0.97	0.40	1.28	1.30	
4.70,37.4	1.00	0.82	0.98	1.86	1.12	2.00	1.00	0.81	0.98	1.83	1.11	2.00	
4.85,37.4	1.11	1.06	1.01	3.38	1.08	1.99	1.11	1.06	1.01	3.34	1.08	1.99	
5.00,37.4	1.18	1.19	1.01	3.90	1.10	1.94	1.17	1.19	1.01	3.85	1.10	1.94	
5.15,37.4	1.19	1.22	1.01	3.73	1.10	1.90	1.18	1.22	1.01	3.67	1.10	1.91	
5.25,37.1	1.17	1.21	1.02	3.40	1.09	1.90	1.17	1.21	1.02	3.34	1.08	1.90	
5.25,36.6	1.17	1.20	1.03	3.50	1.08	1.91	1.16	1.20	1.03	3.42	1.08	1.91	
5.20,36.1	1.18	1.21	1.02	4.71	1.11	1.94	1.17	1.20	1.03	4.57	1.10	1.94	
5.05,35.6	1.11	1.12	1.01	4.10	1.12	2.03	1.11	1.11	1.01	3.97	1.12	2.03	
5.00,35.1	1.06	1.10	1.04	5.64	1.11	1.97	1.06	1.10	1.04	5.50	1.10	1.96	
NEUTRAL ZONE‡: (x(O ⁰) > 50%)													
log R _O =16.3	1.97	2.28	1.02	<u>>100</u>	2.35	2.64	1.97	2.28	1.02	<u>>100</u>	2.35	2.64	
16.7	1.93	2.21	1.01	<u>>100</u>	2.25	2.60	1.93	2.21	1.01	<u>>100</u>	2.25	2.60	
17.0	1.97	2.27	1.02	<u>>100</u>	2.34	2.64	1.97	2.27	1.02	<u>>100</u>	2.34	2.64	
17.3	1.92	2.18	1.01	<u>>100</u>	2.24	2.58	1.92	2.18	1.01	<u>>100</u>	2.24	2.58	
17.7	1.90	2.03	1.01	<u>>100</u>	2.25	2.61	1.90	2.03	1.01	<u>>100</u>	2.25	2.61	
log (T _{*,L_*}) =													
4.55,37.4	0.00	2.27	1.14	<u>>100</u>	2.27	0.00	0.00	2.27	1.14	<u>>100</u>	2.27	0.00	
4.70,37.4	1.77	2.48	1.06	<u>>100</u>	2.39	2.67	1.77	2.48	1.06	<u>>100</u>	2.39	2.67	
4.85,37.4	1.83	2.19	1.02	<u>>100</u>	2.11	2.58	1.83	2.19	1.02	<u>>100</u>	2.11	2.58	
5.00,37.4	1.97	2.27	1.02	<u>>100</u>	2.34	2.64	1.97	2.27	1.02	<u>>100</u>	2.34	2.64	
5.15,37.4	1.93	2.12	1.01	<u>>100</u>	2.25	2.60	1.93	2.12	1.01	<u>>100</u>	2.25	2.60	
5.25,37.1	1.92	2.05	1.01	<u>>100</u>	2.25	2.59	1.92	2.05	1.01	<u>>100</u>	2.25	2.59	
5.25,36.6	1.95	2.02	1.01	<u>>100</u>	2.31	2.65	1.95	2.02	1.01	<u>>100</u>	2.31	2.65	
5.20,36.1	1.91	1.93	1.01	<u>>100</u>	2.24	2.60	1.91	1.93	1.01	<u>>100</u>	2.24	2.60	
5.05,35.6	1.92	1.91	1.01	<u>>100</u>	2.33	2.69	1.92	1.91	1.01	<u>>100</u>	2.33	2.69	
5.00,35.1	1.85	1.80	1.01	<u>>100</u>	2.26	2.65	1.85	1.80	1.01	<u>>100</u>	2.26	2.65	

* Underlined entries indicate that the corresponding lines are very weak or confused by much brighter nearby regions.

† Errors are approximately differences of adjacent rows.

‡ Model truncated at x(H⁺) = 30%. The neutral zone is not complete.

Table 3. Ionic abundances relative to H⁺

Fitted Expression	Fractional error at various temperatures*	Notes
$\text{He}^+ / \text{H}^+ = \text{I}(5876)/\text{I}(\text{H}\beta) 0.739 \left(T/10,000 \right)^{0.231}$	<2%	
$\text{He}^+ / \text{H}^+ = \text{I}(6678)/\text{I}(\text{H}\beta) 2.578 \left(T/10,000 \right)^{0.293}$	<2%	
$\text{He}^{++} / \text{H}^+ = \text{I}(4686)/\text{I}(\text{H}\beta) 0.0832 \left(T/10,000 \right)^{0.233}$	<2%	
$\text{N}^+ / \text{H}^+ = \text{I}(6583)/\text{I}(\text{H}\beta) 1.341 \times 10^{-6} \exp(26,485/T) / (1 + 1.2224 \times 10^{-3} x)$	2% 2% 1% 2%	
$\text{O}^0 / \text{H}^+ = \text{I}(6300)/\text{I}(\text{H}\beta) 4.80 \times 10^{-6} \exp(37,076/T) * (0.383 + 1.2 \times 10^{-4} T - 5.443 \times 10^{-9} T^2)$	1% 1% 1% 1%	1
$\text{O}^+ / \text{H}^+ = \text{I}(3726+3729)/\text{I}(\text{H}\beta) 4.684 \times 10^{-7} \exp(43,706/T) * (1.14 - 1.156 \times 10^{-5} T) * (1.05 + 1.534 \times 10^{-4} n - 2.54 \times 10^{-10} n^2)$	1% 1% 1% 1%	
$\text{O}^+ / \text{H}^+ = \text{I}(7325)/\text{I}(\text{H}\beta) 4.20 \times 10^{-6} \exp(62,545/T) * (0.612 + 0.405 [e^{-z} - \{1.1 - 0.9 \times 10^{-5} T\} e^{+z}]/[e^{-z} + e^{+z}])$, $z = (\log_{10} n - 3.04)$	7% 2% 2% 2%	2
$\text{O}^{++} / \text{H}^+ = \text{I}(5007)/\text{I}(\text{H}\beta) 1.152 \times 10^{-6} \exp(34,609/T) / (1 + 1.2487 \times 10^{-4} x)$	4% 2% 2% 3%	
$\text{Ne}^{++} / \text{H}^+ = \text{I}(3869)/\text{I}(\text{H}\beta) 1.33 \times 10^{-6} \exp(41,250/T)$	3% 2% 1% 1%	
$\text{S}^+ / \text{H}^+ = \text{I}(6717+6731)/\text{I}(\text{H}\beta) 1.660 \times 10^{-7} \exp(25,079/T) * (1.03 + 1.89 \times 10^{-4} n)$	3% 1% 1% 2%	
$\text{S}^{++} / \text{H}^+ = \text{I}(6312)/\text{I}(\text{H}\beta) 3.1 \times 10^{-6} \exp(43,250/T) / (1 + 6.93 \times 10^{-3} x^{0.54})$	2% 2% 2% 2%	
$\text{Ar}^{++} / \text{H}^+ = \text{I}(7136)/\text{I}(\text{H}\beta) 8.189 \times 10^{-7} \exp(24,243/T)$	2% 2% 1% 2%	
$\text{Ar}^{3+} / \text{H}^+ = \text{I}(4740)/\text{I}(\text{H}\beta) 7.433 \times 10^{-7} \exp(29,789/T) * (1 + 0.47e^{-0.0149x})$	1% 1% 1% 1%	
$\text{Ar}^{4+} / \text{H}^+ = \text{I}(7006)/\text{I}(\text{H}\beta) 1.325 \times 10^{-6} \exp(26,279/T) * \left(1.005 + [1.15 \times 10^{-4} n - 0.049] \exp(-0.115 n^{0.39}) \right)$	6% 1% 1% 1%	

* The values of density n and temperature T used in these expressions for ionic abundances should be derived from lines of ions with similar ionization characteristics. $x = n/\sqrt{T}$. Errors in the second column are computed at 7500, 10000, 12500, and 15000 °K, respectively, as described in the text.
Notes to Table 3:

1. The fit is good; however, IONIC is inaccurate owing to the complex form of the target area parameter Ω .
2. The 7325Å line of O⁺ consists of a blend of four lines at 7321.7, 7322.3, 7332.2 & 7332.8 Å.

Table 4. Total abundances relative to H when only optical lines are measured*

i_{CF} Expression	Ref.
$He = He^+ + He^{++}$	
$O = (O^+ + O^{++}) (He / He^+)^{2/3}$	KB
$N = N^+ (O / O^+)$	KB
$Ne = Ne^{++} (O / O^{++})$	KB
$S = (S^+ + S^{++}) [1 - (1 - O^+/O)^3]^{1/3}$ where, if S^{++} is not measurable, adopt $S^{++} = S^+ [4.677 + (O^{++}/O^+)^{0.433}]$	KB
$S = (S^+ + S^{++}) [1.43 - 0.196 (O^{++}/O^+)^{1.29}]$	KAS
$Ar = 1.87 Ar^{++}$ if the only measurable line is [Ar III]	KB
$Ar = 1.34 Ar^{++} (1 + O^+/O^{++})$ if the only measurable line is [Ar III]	F-PBCI
$Ar = (Ar^{++} + Ar^{3+} + Ar^{4+}) (1 - N^+/N)^{-1}$	PLT-P

* In the present paper only the expressions of KB have been adopted.
The [S III]6312Å is assumed to be measurable.